

Skeleton-OOD: An End-to-End Skeleton-Based Model for Robust Out-of-Distribution Human Action Detection

Jing Xu^a, Anqi Zhu^b, Jingyu Lin^a, QiuHong Ke^a, Cunjian Chen^{a,*}

^a*Department of Data Science and AI, Monash University, Melbourne, 3800, Victoria, Australia*

^b*Department of Computing and Information Systems, University of Melbourne, Melbourne, 3052, Victoria, Australia*

Abstract

Human action recognition is crucial in computer vision systems. However, in real-world scenarios, human actions often fall outside the distribution of training data, requiring a model to both recognize in-distribution (ID) actions and reject out-of-distribution (OOD) ones. Despite its importance, there has been limited research on OOD detection in human actions. Existing works on OOD detection mainly focus on image data with RGB structure, and many methods are post-hoc in nature. While these methods are convenient and computationally efficient, they often lack sufficient accuracy, fail to consider the exposure of OOD samples, and ignore the application in skeleton structure data. To address these challenges, we propose a novel end-to-end skeleton-based model called Skeleton-OOD, which is committed to improving the effectiveness of OOD tasks while ensuring the accuracy of ID recognition. Through extensive experiments conducted on NTU-RGB+D 60, NTU-RGB+D 120, and Kinetics-400 datasets, Skeleton-OOD demonstrates the superior performance of our proposed approach compared to state-of-the-art methods. Our findings underscore the effectiveness of classic OOD detection techniques in the context of skeleton-based action recognition tasks, offering promising avenues for future research in this field. Code is available at <https://github.com/YilliaJing/Skeleton-OOD.git>.

*Corresponding author: Tel.: +86 1-517-303-2723;
Email address: cunjian.chen@monash.edu (Cunjian Chen)

1. Introduction

Human-centric visual understanding enhances the development of intelligent machines, enabling humans to accomplish greater tasks and improve their quality of life. Deep learning-based models have shown remarkable performance in supervised human action classification tasks. In skeleton-based human action datasets, this task can be solved as a typical spatio-temporal modeling problem [1, 2, 3]. Although these methods have achieved high accuracy in supervised classification problems, they still lack consideration for out-of-distribution (OOD) issues. An important assumption in these approaches is that the distribution of the training set is similar to that of the test set. However, this can not always be achieved in practice. When straightly applying these action recognition models to recognize samples outside the distribution of the training dataset, they may exhibit overconfidence by selecting a category from the known distribution [4]. Hence, it is essential for such models to be aware of the boundaries of learning for safety concerns [5], ensuring the robustness of computer vision systems. How to deal with this OOD detection problem has attracted widespread attention in fields such as autonomous driving [6] and medical image analysis [7].

Works in OOD detection focus on OOD samples caused by semantic shift, aiming to determine whether a sample belongs to a category included in the training dataset. This task presents two challenges: quantifying the differences between in-distribution (ID) and OOD samples and distinguishing them based on their expressions. For the first challenge, one typical approach is score measuring methods [8], such as the softmax confidence score [8]. Inputs with low softmax confidence scores are classified as OOD. However, neural networks can produce arbitrarily high softmax confidence scores for inputs far from the training data [9]. To address this, the energy score is proposed for OOD detection. It can be derived from a purely discriminative classification model without explicitly relying on a density estimator. Experiments have shown that it outperforms softmax-based score measuring methods.

Based on such score measuring methods, a crucial issue is how to maximize the difference in score distributions between OOD and ID samples. To achieve this, difference amplification methods [10, 11] have been designed. However, these methods are mostly implemented in a post-hoc manner, meaning the model itself cannot inherently distinguish OOD samples. This does not fundamentally solve the problem of ‘letting the model know what

it knows’. Furthermore, these methods were originally designed for OOD detection in RGB-structured datasets. Their effectiveness in handling action recognition problems with skeleton structure data has not yet been investigated.

Furthermore, methods like [12, 13] have attempted to achieve this goal by introducing OOD-related information into the training stage. However, in practice, we cannot measure the specific categories of OOD. Similarly, when the OOD category itself expands, the overconfidence problem still remains. In summary, while these methods significantly improve the accuracy of OOD recognition, achieving this goal using an end-to-end framework without prior OOD information remains challenging.

To address the limits and challenges mentioned above, we propose an end-to-end model called Skeleton-OOD to deal with the out-of-distribution detection problem for skeleton-based action recognition. Considering that the state-of-the-art feature extractors for supervised ID classification are well-developed, we focus on exploiting the extracted features to extend their adaptability for OOD detection while maintaining robust prediction performance for ID classification. We input graphs, joints, and temporal sequences into the spatial-temporal feature extractor to obtain feature embeddings as output. Based on this, we first creatively applied a feature activation module that utilizes ASH [14] to project the original features for fitting OOD detection in the training stage. Specifically, it filters useless information and amplifies the key feature dimensions to generate a more sensitive and accurate representation of abnormal detections. However, in its original work, the activation method was only used in a post hoc manner after the trained model, and the energy score was only used for judgment. Then, regarding this as an orthogonal aggregation to the original features, we innovatively designed a feature fusion module, which integrates the original backbone outputs and the OOD-targeted activated features to enable the model to preserve a strong recognition ability for ID data while also nicely discriminating the potential OOD existences. To support the framework with end-to-end training, we suggested a meticulously designed learning loss that combines the energy function and cross-entropy information. This approach aims to improve the model’s understanding of the energy score distribution in ID data, thereby further benefiting the accurate detection of OOD samples.

Our main contributions are summarized as follows:

- We propose Skeleton-OOD, an end-to-end skeleton-based OOD detec-

tion model that addresses overconfidence by solely training on ID data.

- The attention-based feature fusion block is designed to enhance OOD detection accuracy while preserving classification ability for ID classes.
- We design an energy-based loss function, which can improve score differentiation between ID and OOD samples, thus effectively maximizing their distribution separations.
- The proposed model Skeleton-OOD outperforms baselines on NTU-RGB+D 60, NTU-RGB+D 120, and Kinetics-400 datasets in the human action OOD detection task.

The rest of the paper is organized as follows: Section 2 explains basic knowledge of skeleton-based action recognition tasks with GCNs and the theory of why energy score is most widely used in OOD detection. Section 3 introduces our proposed method in detail, including the proposed framework, feature fusion block, and loss function design. Section 4 mainly discusses the results of experiments and thus shows the effectiveness and usability of our proposed model. We offer conclusions, limitations, and future works in Section 5.

2. Related works

2.1. GCNs for Skeleton-based Action Recognition

Human action recognition tasks are a typical problem in computer vision, which have wide applications in the real world, including human-computer interaction [15] and video surveillance [16]. Skeleton-based methods have their unique advantages. The skeleton structure can provide more accurate node-level information and ignore the influence of background noise, thus improving the prediction accuracy of recognition.

In the early phases of skeleton-based action recognition using deep learning methods, convolutional neural networks (CNNs) [17, 18, 19], and recurrent neural networks (RNNs) [20, 21] were commonly utilized. However, these approaches had limitations as they didn't fully leverage the structural arrangement of the joints.

Subsequently, researchers built spatio-temporal architectures to handle this problem. Many works use handcrafted physically connected (PC) edges among human skeletons to extract spatial features [2, 3], and GCNs can

handle this type of graph-structured data very well. The graph defined on the human skeleton is denoted as $G(V, E)$, with V representing the joint group and E representing the edge group. The representation of 3D time-series skeletal data is denoted as $X \in \mathbb{R}^{c \times t \times |V|}$, where $|V|$ represents the number of joint nodes, c is the number of channels, and t denotes the temporal window size. The operation of GCN with an input feature map X can be described as follows:

$$\mathbf{F}_{\text{out}} = \mathbf{A}\mathbf{X}\Theta. \quad (1)$$

Here, Θ denotes the pointwise convolution operation. The adjacency matrix A , which is initialized as $\Lambda^{-\frac{1}{2}}\mathbf{A}\Lambda^{-\frac{1}{2}} \in \mathbb{R}^{N_g \times |V| \times |V|}$, where Λ is a diagonal matrix for normalization, and $N_g = 3$ in experiments.

However, relying solely on PC edges for spatial relationships is insufficient, as it limits the receptive fields due to their heuristic and fixed nature [22]. Additionally, the varying contributions of each edge must be considered, as the importance of joints in different body parts varies for specific actions. To address these issues, Hierarchically Decomposed Graph Convolutional Networks (HD-GCN) [23] were proposed. The graph convolution operation of HD-GCN is defined as:

$$\mathbf{F}_{\text{out}} = \sum_{g \in G} \mathbf{A}_g \mathbf{X} \Theta_g, \quad (2)$$

where $G = \{g_{pc}, g_{sl}, g_{fc}\}$ denotes three graph subsets, and g_{pc} , g_{sl} , and g_{fc} indicate physical connections, self-loops, and fully connected joint subsets, respectively. It represents three typical useful graph relationships to help explore spatial relationships between joints. The construction of these three types of subsets will be introduced in detail in section 3.1. With this operation, HD-GCN achieved an average Top-1 accuracy of 93.9% across three experimental datasets.

2.2. Methods for out-of-distribution detection

Research on out-of-distribution detection can be mainly categorized into two ways. First, we can define a scoring function that maps each input point to a single scalar, such that in-distribution and out-of-distribution data will have different distributions. Thus, we can identify the out-of-distribution samples by calculating this score. There are many works about how to define this kind of score for pre-trained neural networks. [8] proposed the maximum

predicted softmax probability (MSP). After that, [12] proved that the log of the MSP was equivalent to a special case of the free energy score. This indicates that there are some cases in ID and OOD data with similar MSP values but different energy scores. As a result, energy score has become one of the most widely used score measuring methods.

Secondly, we can distinguish ID and OOD by trying to modify the feature captured by a pre-trained neural network in a post-hoc way, which is usually applied to feature activations. Numerous experiments have shown that different feature activation methods can help differentiate ID and OOD. [10] proposed rectified activation (ReAct) after observing that OOD data can trigger unit activation patterns that were significantly different from ID data in the penultimate layer of the model. Performing truncation can help drastically improve the separation of ID and OOD data. [11] found that some operations similar to Batch Normalization might increase the difference in scores (e.g., MSP and energy score) between ID and OOD data. DICE [24] was proposed to address the shortcomings of redundant information expressed in the high space of neural networks. It attempted to define weights (i.e., weight \times activation) to sort and filter the nodes in the penultimate layer of the neural network for denoising. This further reduces the variance value of the ID and OOD data score distributions, making it easier to separate the peaks of the two distributions. Similar to the previous works, [14] removed the top-K elements (usually a large portion over 50%) and adjusted the remaining (e.g. 10%) activation values by scaling them up or straightly assigned them a constant number. It achieves state-of-art performance on several benchmarks of image classification.

However, most of the first two kinds of methods are considered post-hoc. While they can reduce calculation costs than training another new specific OOD detection model, research by [25] showed that they were still less competitive than some works that utilized OOD information in the training stage, such as works by [26] and [27]. Additionally, these methods were initially designed for OOD detection in RGB-structured datasets. Their effectiveness in addressing action recognition problems with skeleton structure data has not yet been explored. In this work, we prove the validity of these methods on skeleton-based datasets and then take steps to solve these problems.

2.3. Energy-based out-of-distribution detection

In deep neural networks, out-of-distribution detection distinguishes samples that deviate from the training distribution. In this work, we only focus

on the standard OOD detection that concerns semantic shifts, in which OOD data is defined as test samples from semantic categories that were not seen during training. Ideally, the neural network should be able to reject such samples as OOD while maintaining strong classification performance on ID test samples belonging to seen training categories [28]. To achieve this goal, a common approach is to utilize the data density function, denoted as $p^{in}(x)$, and identify instances with low likelihood as OOD. Nevertheless, prior studies have demonstrated that density functions estimated by deep generative models are not consistently reliable for OOD detection [5].

Energy-based out-of-distribution detection employs the energy score for detection, where the difference of energies between ID and OOD facilitates separation. The energy score addresses a crucial issue associated with softmax confidence, which can lead to excessively high values for OOD examples [29].

Let us define a discriminate neural network $f(x) : \mathbb{R}^D \rightarrow \mathbb{R}^K$, which maps the input x to K real-valued numbers known as logits. Its energy score function $E(x, f)$ over \mathbb{R}^D with softmax activation can be defined as follows:

$$E(\mathbf{x}; f) = -\varepsilon \cdot \log \sum_i^K e^{f_i(\mathbf{x})/\varepsilon}, \quad (3)$$

where ε is the temperature parameter. It can also be proved that a model trained with negative log-likelihood (NLL) loss will push down energy for in-distribution data points and pull up for other labels [30]. Since cross-entropy loss can be implemented as NLL loss after the logSoftmax function, it will also push down the energy score of ID data. In other words, the ID sample will have a larger negative energy score $-E(x; f)$ than the OOD sample.

3. Method

Our goal is to achieve accurate human action OOD detection through an end-to-end framework without any other subsequent fine-tuning or post-hoc operations. The whole framework of the proposed skeleton-based OOD human action detection model is shown in Figure 1.

It can be divided into three main steps of the end-to-end Skeleton-OOO framework: Firstly, a GCN-based backbone is employed to extract features from skeleton data. Secondly, The extracted features are then activated and fused with the original ones. The function of the feature fusion block is to

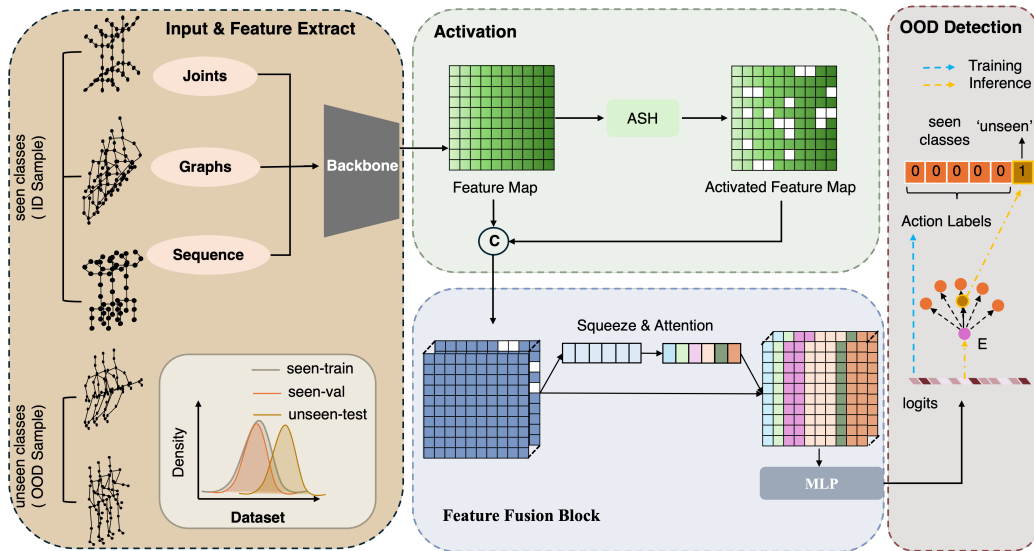


Figure 1: Framework of the proposed Skeleton-OOD model. The symbol \odot represents the vector concatenate operation.

improve the recognition ability of OOD samples while preserving the original classification performance of ID data. Finally, it is fed into the classifier, and OOD detection is performed based on the classifier output logits as shown in Figure 4. Besides, the whole model is trained by our newly designed energy-based loss function. In the following sections, we will provide a detailed discussion of each component.

3.1. GCN-based feature extractor

Since many GCN-based models have achieved great success in action recognition tasks, in this work we use existing models that perform best in ID data classification to extract embeddings from human skeleton data. It is an important step for a GCN-based model to construct the graph topology in advance. A topology can bring great convenience to the spatial learning of the model while incorporating prior information thus improving the physical consistency of the model. Following the previous work by [23], we define three types of edges for joint connections, while keeping the number of nodes unchanged (see Figure 2).

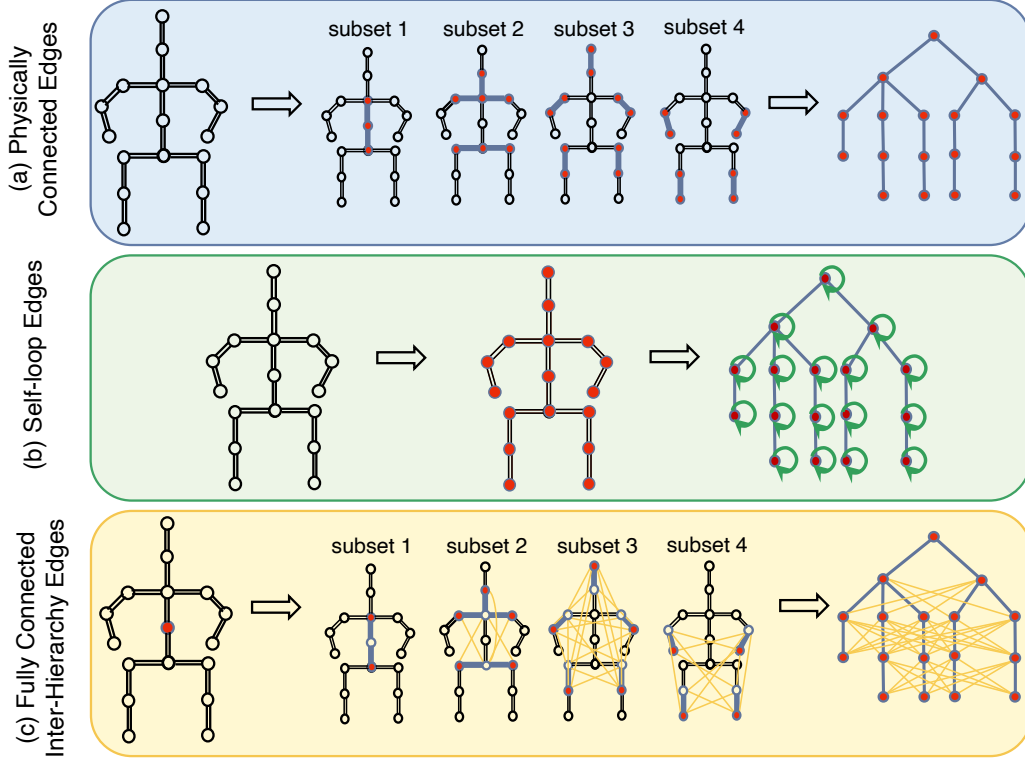


Figure 2: Description of the graph construction method. (a) Physically connected edges. The nodes and edges marked in each subset correspond to the nodes and edges of the two adjacent layers of nodes in the rightmost tree structure. (b) Self-loop edges (green arrow pointing to the joints themselves). We add self-loops of each joint to help the model take into account the characteristics of the joints themselves when conducting graph convolution. (c) Fully connected inter-hierarchy edges. We assume that the inter-hierarchy relationships in each subset can help to distinguish different actions. Thus, we add fully-connected edges in each subset as shown in yellow lines.

Let us define $G = \{g_{pc}, g_{sl}, g_{fc}\}$ as the three types of graph. The first type of graph g_{pc} is physically connected edges, which are represented by blue lines between joints in Figure 2 (a). It represents the natural physical relationships in skeleton data. The second type g_{sl} is the self-loop, where nodes are connected to themselves. By incorporating self-loops, nodes are enabled to consider their own features during message passing in addition to relying on neighboring nodes' information, which helps stabilize the training process. Additionally, self-loops can be regarded as a regularization mecha-

nism to prevent over-fitting, making them a commonly used method in graph neural network construction[31].

The third type of graph is a hierarchical fully connected graph g_{fc} . We employ a balanced tree approach to reconstruct the graph structure (as illustrated on the right side of Figure 2). Fully connected edges are constructed between adjacent nodes across two levels of the balanced tree, based on the hierarchical level of the nodes. This approach considers that the characteristics of actions may correlate with features across various levels of the body’s hierarchical structure. Moreover, it expands the model’s receptive field spatially in the feature space, enhancing the model’s generalization ability. This approach has been widely proven to be effective in previous experiments. After that, for the input skeleton joints data X , graph subsets G and temporal sequence T , the output feature maps F are obtained as follows:

$$F = f^{HD-GCN}(X, G, T). \tag{4}$$

3.2. Feature activation shaping and fusion

Following the previous work [14], we utilize activation shaping (ASH) operation to filter out useless information in high-dimensional HD-GCN captured feature maps F , which can bring benefits to other downstream tasks (e.g. OOD detection). However, the difference is that we utilize it in the training stage to help the model itself distinguish OOD samples.

There are three types of ASH strategies: ASH-P, ASH-B, and ASH-S. As shown in Figure 3, for the input feature maps F , ASH-P only sets values less than t into zero, ASH-B resets the non-zeros by binarization, and ASH-S sets them with scaling. Details of these three strategies can be found in Appendix A. The difference among them lies in the normalization strategies after pruning. In the experimental part, we show the results of all these three strategies in training. After that, we retain both the output feature maps and the pruning features:

$$\hat{F} = [F, ASH(F)], \tag{5}$$

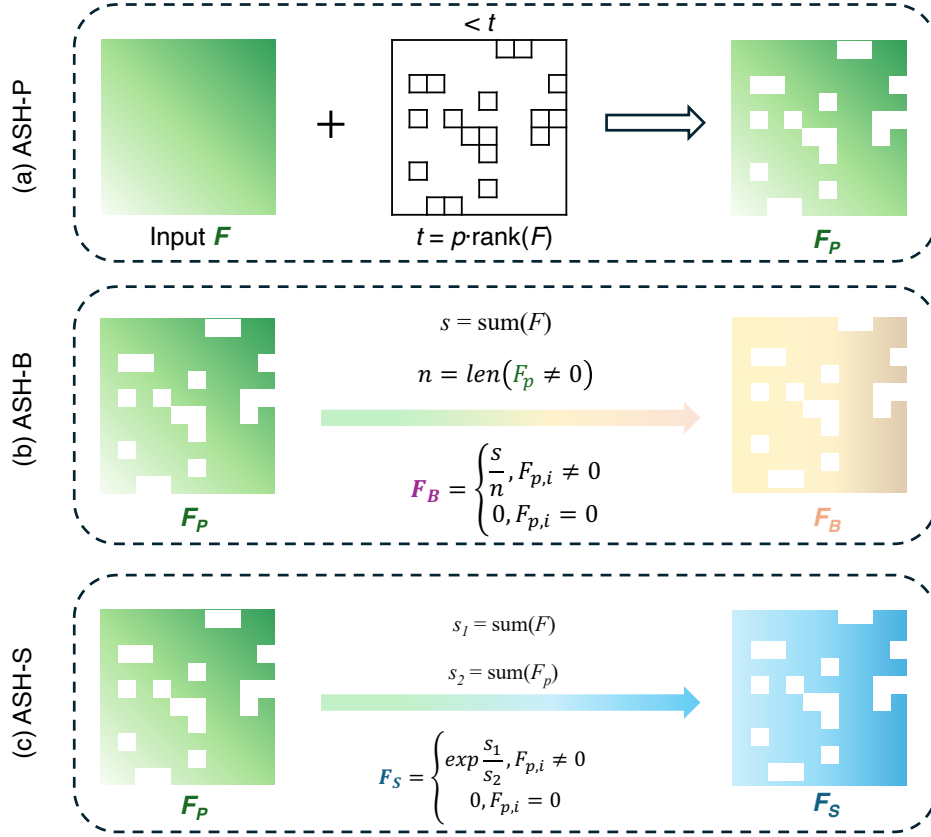


Figure 3: Process of Activation Shaping strategies. They prune the elements by pruning percentages and then conduct different strategies to assign values to the remaining elements.

where $\text{ASH}(F)$ represents the results of any activation strategy acting on the feature maps F , and $[\cdot, \cdot]$ denotes the process to concatenate two vectors into a single one. The concatenated features undergo two main operations in the feature fusion process: one SE layer [32] primarily aimed at enhancing the model’s sensitivity to channel features:

$$F^{SE} = \hat{F} \cdot \text{ReLU} \left(W_{fc} \cdot \underbrace{\frac{\sum_i^{k_h} \sum_j^{k_w} \hat{F}}{k_h \times k_w}}_{\text{average pool}} + b \right), \quad (6)$$

and the other MLP layer [33]:

$$F^{fuse} = \text{MLP} (F^{SE}). \quad (7)$$

Here, W_{fc} represents the learnable weights. At this stage, we have acquired the fused feature F^{fuse} . Experiments show that it can improve the recognition ability of unseen classes while ensuring the classification accuracy of seen classes.

3.3. OOD detection using logits

After the feature pruning and fusion process, the extracted features will be fed into a classifier:

$$\text{logits} = W'_{fc} \cdot \text{drop_out} (F^{fuse}) + b'. \quad (8)$$

Here Eqn. 8 shows the classification operation after data fusion, and W'_{fc} is the learnable weight. Then we get the logits ready for the downstream OOD detection task. The logits' dimension equals the number of seen classes plus one unseen class. The detailed process of OOD detection is illustrated in Figure 4.

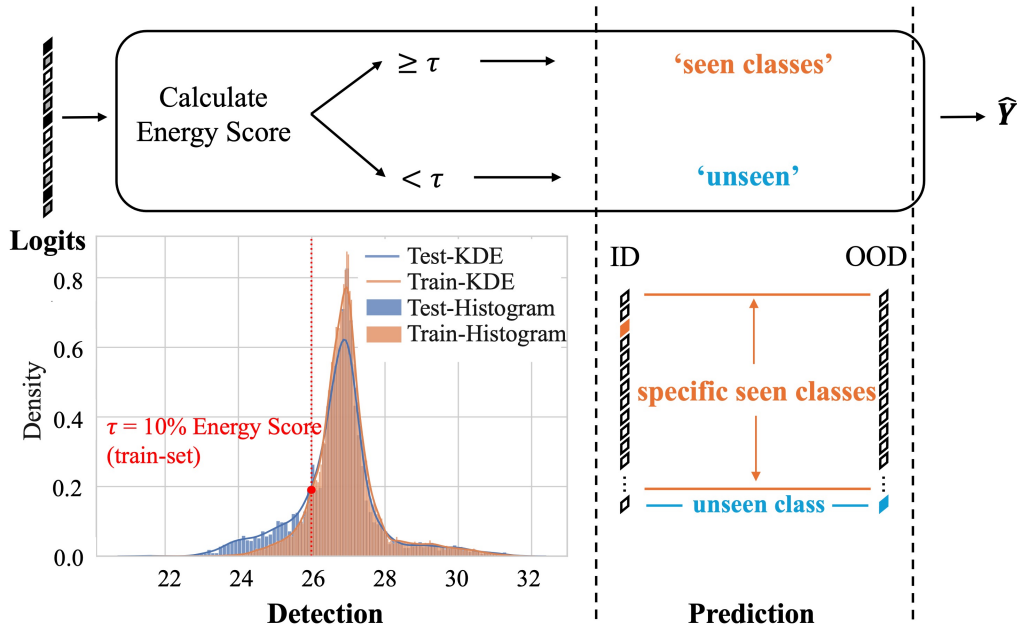


Figure 4: Explanation of OOD detection process. In the detection stage, the input is the logits from the previous feature extractor. Based on the Energy-based theory, the lower the score, the more likely the sample is the in-distribution.

For the input logits after the classifier, we measure the energy score of each sample using Eqn. 3: If the score is smaller than τ , we will recognize it as ‘unseen’ for OOD and set the element value representing the probability that the sample belongs to the unknown category to 1. Otherwise, the probability of unseen will remain 0, and others (representing specific seen classes) will be the value between 0 to 1. The output of this stage will be multi-classes. The value of parameter τ is given based on the top 10% of energy scores on the training set. The assumption behind this is that the energy score of OOD after training is less than the energy score of 90% ID data. After that, we can get a vector \hat{Y} that represents the probability that the sample belongs to each class.

Algorithm 1 Skeleton-OOD Detection Algorithm

Input: Action skeleton data X ;

Graph structure $G = \{g_{id}, g_{cf}, g_{cp}\}$;

Detection threshold τ from training stage;

Algorithm running STAGE;

Output: Predict action label \hat{Y} for inference or value of loss function L in the training stage.

```

1:  $F = f^{HD-GCN}(X, G, T)$                                 ▷ extract feature maps
2:  $\hat{F} = [F, ASH(F, p)]$                                     ▷ feature fusion block
3:  $F^{SE} = SELayer(\hat{F})$                                   ▷ detailed in Eqn. 6
4:  $F^{fuse} = MLP(F^{SE})$ 
5:  $logits = Classification(F^{fuse})$                        ▷ detailed in Eqn. 8
6: if STAGE == ‘train’ then
7:   return  $L(logits)$                                      ▷ detailed in Eqn. 9
8: else
9:    $score = -E(logits)$                                    ▷ calculate energy score
10:  if  $score \geq \tau$  then
11:     $logits[-1] = 1$                                      ▷ detect as OOD
12:  end if
13:   $\hat{Y} = argmax(softmax(logits))$                        ▷ get label through the normalized
    one-hot vector
14:  return  $\hat{Y}$ 
15:  Calculate evaluation metric.
16: end if

```

3.4. Energy-based loss function

As stated in section 2.2, although the model trained with cross-entropy loss will lower the energy score value of OOD data, the gap between the two distributions may not always be optimal for detection. Therefore, we propose an energy-bounded learning objective and combine it with traditional cross-entropy loss:

$$L = - \sum_{logits_{in}} P(logits_{in}) \log f(logits_{in}) + \alpha \cdot \mathbb{E}_{(logits_{in}, y) \sim \mathcal{D}_{in}^{train}} (\max(0, E(logits_{in}) - m_{in}))^2. \quad (9)$$

The first part is the cross-entropy part, where $P(logits_{in})$ is the expected probability output, and $f(\cdot)$ represents the model output on in-distribution training data. The second part is energy-based, where \mathcal{D}_{in}^{train} is the in-distribution training data, $E(logits_{in})$ represents the energy score of in-distribution data, m_{in} is the margin parameter which is set before can help the ID energy score distribution reduce the variance and close to this point, α is the tuning parameter that adjusts the proportion of energy part. With the help of this learning objective, the variance of ID data will be reduced. We can also ensure the model understands the energy score distribution of ID data, thus indirectly having the ability to distinguish ID and OOD samples. The overall process can be found in Algorithm 1.

4. Experiments

To demonstrate the human action detection accuracy of our proposed model Skeleton-OOD, a series of experiments are conducted. In this section, we elucidate the intricate details of the experimental design and present a thorough analysis of the experimental results. First, we introduce three datasets and describe their data pre-processing methods. Subsequently, we compare our work with other existing OOD detection methods and identify the proposed model’s strengths and weaknesses. Finally, we design three ablation studies to examine the effectiveness of individual modules.

4.1. Dataset description

- **NTU-RGB+D 60 [34] & 120 [35]** ¹: The NTU-RGB+D 60 dataset (NTU60), comprising 60 motion categories and 56,880 video samples, is extensively employed in diverse action recognition tasks. The NTU-RGB+D 120 dataset (NTU120) is an extension of the NTU-RGB+D 60 dataset, expanding the total number of human action categories to 120. Both datasets encompass five data modalities: 3D skeletons (body joints), masked depth maps, full-depth maps, RGB videos, and IR data. In this study, we exclusively utilize the 3D skeleton sequence data. The 3D skeleton data includes the 3D coordinates (X, Y, Z) of 25 body joints per frame for a maximum of two subjects. The actions in these datasets are categorized into three main groups: daily actions, interactive actions, and medical conditions. 5 classes are randomly selected as unseen from the NTU60 dataset and ten classes from the NTU120 dataset. Note that these unseen categories encompass samples from each of the three groups. Before splitting, we cleaned and preprocessed the raw dataset following the prior work [23].
- **Kinetics human action dataset (Kinetics 400) [36]**: It is, by far, the largest unconstrained action recognition dataset created by DeepMind. It covers 400 action classes, ranging from human-object interactions to human-human interactions, and also includes other complex interactions from YouTube videos. Since the Kinetics dataset provides only raw video clips without skeleton data, we adopt the skeleton-based action data processed by previous work STGCN ² [1]. The processed data sequences contain 18 joints and 2 subjects. We randomly select 33 action classes marked as ‘unseen’ for OOD samples, ensuring the same ratio as used in the NTU60 and NTU120 datasets.
- **Dataset splitting protocol**: Both the training set and validation set consist of data with known labels. In this work, we create two types of test dataset: ID-only (randomly selected from known classes) and ID-OOD mix dataset, for the aim of testing the model’s ability to classify ID samples and distinguishing OOD samples (all samples of unknown classes) from mixed samples. The seen class data in the validation set

¹<https://rose1.ntu.edu.sg/dataset/actionRecognition/>

²<https://github.com/yysijie/st-gcn>

and the ID-only test set are consistent. The data volume ratio of the training set and ID-only test set/validation set in the known class data is 9:1. The number of samples in the train, validation, and test dataset is shown in Table 1.

Table 1: Number of samples in different data sets.

Dataset	Train	Val	Test (seen/unseen)
NTU60	46,898	5,184	5,184/4,730
NTU120	94,553	10,447	10,447/9,467
Kinetics400	216,441	24,049	24,049/19,742

4.2. Experiment details

4.2.1. Experiment settings

- Implementation details:** We adopt HD-GCN [23] as the backbone to extract graph-structured skeleton data as shown in Figure 1. The batch size of data is 64. The SGD optimizer is employed with a Nesterov momentum of 0.9 and a weight decay of 0.0004. Due to the differences in dataset size and data characteristics, we also used some different hyperparameters when training on different datasets: The hidden layer dimension of MLP is 400 for NTU and 576 for Kinetics. The learning rate is 0.001 for NTU60 and NTU120, and 0.01 for Kinetics400. The number of learning epochs is set to 100 for NTU60 and NTU120, and 150 for Kinetics400, with a warm-up strategy [37] applied to the first five epochs for more stable learning. The model used in this study contains a total of 1,815,060 parameters, leading to a trained model file size of approximately 9.3 MB. The training process for this model is efficient, with each epoch requiring about 7 minutes on the NTU60 dataset. The test on the NTU60 ID-OOD mix dataset (containing 9,914 samples) takes 14 seconds in total. All our experiments are conducted on NVIDIA GeForce RTX 3090, CUDA 11.6 + PyTorch 1.12.1.
- Evaluation metric:** As depicted in Figure 4, we assess both the accuracy of detecting unseen samples and classifying seen samples. All samples under evaluation first undergo a threshold-based determination to discern whether their labels are unseen. If classified as ‘unseen’, they are marked accordingly; otherwise, they are predicted to belong to known categories. Regarding the unseen detection task, it

can be viewed as a binary classification problem. We evaluate its accuracy using Detection Error [38], AUROC [39], and FPR at 95% TPR [38], following the methodology outlined in [40]. For action recognition tasks involving seen data, we employ Top-1 Accuracy [23] for quantitative evaluation. The details of these evaluation metrics are outlined as follows:

- 1) **Detection Error (Error)** [38]: It measures the misclassification probability when the True Positive Rate (TPR) is 95%. The definition of an Error is:

$$Error = 0.5 \times (1 - TPR) + 0.5 \times FPR, \quad (10)$$

where FPR stands for False Positive Rate.

- 2) **AUROC** [39]: It stands for the Area Under the Receiver Operating Characteristic (ROC) curve, which depicts the relation between TPR and FPR and ranges from 0 to 1 (the larger the value, the higher the accuracy). AUROC provides a single scalar value that summarizes the overall performance of a binary classifier across all possible thresholds.
- 3) **FPR at 95% TPR (FPR95)** [38]: It refers to the rate of false positive predictions when the true positive rate reaches 95% in a classification task.
- 4) **Top-1 Accuracy (ACC)** [23]: It measures the proportion of correctly predicted instances among all instances, where the predicted class label exactly matches the ground truth label for each instance. It is defined as:

$$ACC = \frac{hit}{N} \times 100\%, \quad (11)$$

where hit means the number of samples that were predicted correctly, and N represents the total number of test samples.

- 5) **Overlap**: For most energy-based OOD detection, the overlapping portion of the score distributions of ID and OOD indicates that OOD data is missed or ID data is misjudged as OOD. The smaller the overlap area of the two distributions, the greater the distinction between the two data. Therefore, we propose to use the distribution overlap area for evaluation, which can more intuitively reflect the error of OOD recognition.

- **Loss function:** As introduced in section 3.3, we design a novelty energy loss to help the model distinguish OOD data during the training stage using only ID data. We set $\alpha=0.1$ and $m_{in}=-25$ in Eqn. 9.

4.2.2. Baselines

Since most OOD detection models are post-hoc methods, we retain basic feature extraction parts and change different post-hoc methods to achieve OOD detection. We compare the proposed Skeleton-OOD with four main methods: one score measuring method MSP (**M**aximum **S**oftmax **P**robability) [8] and three different feature activation methods – ReAct (**R**ectified **A**ctivation) [10], DICE (**D**irected **S**parisification) [24], DICE+ReAct, ASH (**A**ctivation **S**haping) [14]. Details are shown below:

- **MSP (Maximum Softmax Probability):** [8] claims that out-of-distribution examples tend to have lower maximum softmax probabilities than known samples. This scoring-based method has shown wide success in the computer vision area.
- **ReAct (Rectified Activation)** [10]: A post-hoc method was proposed to reduce the overconfidence problem of the model on OOD data by truncating activations on the penultimate layer of a network to limit the effect of noise.
- **DICE (Directed Sparisification)** [24]: Another post-hoc method, based on the idea of denoising useless information, sorts the weights of its contribution (i.e., weight \times activation). It claims that only a subset of units contributes to the in-distribution prediction results. However, it will result in non-negligible noise signals when measuring out-of-distribution data.
- **DICE + ReAct:** Following previous work [14], we construct a baseline that filters out noise signals using both DICE and ReAct methods.
- **ASH (Activation Shaping)** [14]: It consists of three different mechanisms to conduct pruning-based feature activation shaping, including ASH-P, ASH-S, and ASH-B.

4.2.3. Ablation study

To verify the effectiveness, we design ablation studies on the following components of Skeleton-OOD.

- **GCN**: This is designed to measure the effect of the feature fusion block of Skeleton-OOD. As previously mentioned, Skeleton-OOD has two parts features: GCN-based features, which excel in classifying in-distribution (ID) samples, and ASH-based features, which aim to reduce overconfidence in predictions for OOD samples. This experiment can prove the improvement effect of ASH operation on the model OOD recognition task.
- **ASH**: Based on the analysis of previous work, a pruning strategy that solely relies on thresholding may prove inadequate in certain scenarios, thus affecting the OOD recognition effect of the model. To verify whether such a problem also exists in unseen action detection, and to illustrate the role of the feature fusion module, we design such an ablation study experiment.
- **CE Loss**: To demonstrate the effect of the proposed energy loss function, we conduct experiments by training with conventional CE loss only.

Except for these, we also explored the results of replacing another backbone as feature extractors and another loss function for training.

4.3. Results and discussion

4.3.1. Performance comparison against baselines

We evaluate the proposed Skeleton-OOD method against baselines across three datasets for two tasks: (a) to distinguish OOD samples from an ID and OOD mixture dataset, and (b) to evaluate whether ID samples will be misclassified as OOD merely based on ID data. We also provide the average results for all models involved across the three datasets.

As seen from Table 2, our method achieves the best performance in most metrics on the OOD test dataset. **On the NTU60 dataset, our method achieves an average AUROC of 85.57% for OOD detection, with the accuracy of seen classification exceeding 91% in Table 3.** Compared with several post-hoc methods, the average AUROC increases by 43.48%. Based on the average results on the three data sets, our method achieves the best on almost all indicators (FPR95 and AUROC). To some extent, our method alleviates the problem of overconfidence in the trained model when facing OOD samples using only an end-to-end model.

Table 2: Comparing the results of the OOD recognition task with other methods on the ID-OOD mix test dataset. The best results are shown in bold.

OOD Methods	NTU60			NTU120			Kinetics400			Average		
	Error ↓	FPR95 ↓	AUROC ↑	Error ↓	FPR95 ↓	AUROC ↑	Error ↓	FPR95 ↓	AUROC ↑	Error ↓	FPR95 ↓	AUROC ↑
MSP	38.58	72.16	84.25	50.00	59.69	86.94	50.00	92.82	46.28	46.19	74.89	72.49
ReAct	49.99	80.29	59.79	50.00	99.60	37.98	51.19	95.88	47.65	50.39	91.92	48.47
DICE	52.47	99.95	35.62	24.24	56.40	84.84	51.12	96.16	46.34	42.61	84.17	55.60
D+R	52.49	100.00	30.80	50.00	99.60	37.98	51.19	95.88	47.66	51.23	98.49	38.81
ASH-P	26.87	58.33	84.48	21.12	56.78	86.20	50.16	92.55	46.75	32.72	69.22	72.48
ASH-S	50.00	59.77	78.73	50.00	60.72	85.46	51.22	95.74	48.82	50.41	72.08	71.00
ASH-B	42.72	78.77	68.43	49.99	58.53	85.96	51.11	96.25	46.72	47.94	77.85	67.04
Ours	30.42	52.68	86.64	21.36	60.64	86.40	51.37	90.61	50.43	34.38	67.98	74.49
ASH-P												
Ours	33.72	62.45	84.10	37.87	59.67	85.09	50.37	93.67	48.23	40.65	71.93	72.47
ASH-S												
Ours	30.21	55.43	85.98	19.57	56.11	87.17	51.25	95.62	47.17	33.68	69.05	73.44
ASH-B												

For the ID sample-only evaluation in Table 3, the best accuracy in ID multi-class classification may sometimes be achieved by other methods, especially in the NTU60 dataset. However, these methods show poor performance in OOD detection tasks (see Table 2), which means that the model still recognizes most of the data as ID. Consequently, the issue of overconfidence persists. Nevertheless, based on the average performance of the three data sets, our method still obtains the highest classification accuracy in the ID sample-only test. In summary, our method maintains the accuracy of ID data classification while also ensuring effective detection capability for OOD tasks. This phenomenon may result from ASH-P’s zero-or-not mechanism. Our analysis indicates that, with the energy-based loss function, ASH-P produces a more pronounced peak in the energy-score distribution for ID samples and a narrower range, as seen in Figure 5 (d). In contrast, the ASH-B and ASH-S methods fill in the none-zeros with the designed “averaged” values, making it harder for the model to distinguish irrelevant information during training.

At the same time, by comparing the results of the three activation methods of our model horizontally, the performance of the three methods on different data sets has its advantages and disadvantages. As can be seen from Table 2, in the OOD detection task, ASH-P and ASH-B perform better in most indicators. When considering the average performance across all three datasets, the ASH-P activation method demonstrates better dataset transferability and greater stability. From Table 3, our method performs more prominently on the NTU120 and Kinetics data sets on ID data, especially under the activation of ASH-P and ASH-B methods. Judging by the number of top-performing indicators across the three datasets and the aver-

Table 3: Comparing the results of the ID multi-class classification task with other methods on the ID-only test dataset. The best results are shown in bold.

ID-only	NTU60		NTU120		Kinetics400		Average	
Methods	Top1 \uparrow	Overlap \downarrow	Top1 \uparrow	Overlap \downarrow	Top1 \uparrow	Overlap \downarrow	Top1 \uparrow	Overlap \downarrow
MSP	91.69	0.35	89.64	0.41	22.39	0.88	67.91	0.55
ReAct	88.27	0.83	83.82	0.80	20.98	0.95	64.36	0.86
DICE	94.23	0.72	76.29	0.47	21.37	0.93	63.96	0.71
D+R	92.76	0.67	47.54	0.78	20.37	0.95	53.56	0.80
ASH-P	91.32	0.45	88.91	0.43	25.18	0.92	68.47	0.60
ASH-S	91.39	0.55	89.35	0.45	23.84	0.98	68.19	0.66
ASH-B	89.69	0.73	88.98	0.42	20.81	0.94	66.49	0.70
Ours ASH-P	91.94	0.39	89.84	0.40	26.18	0.89	69.32	0.56
Ours ASH-S	91.22	0.42	88.98	0.43	23.22	0.90	67.81	0.58
Ours ASH-B	91.61	0.41	89.13	0.39	25.04	0.95	68.59	0.58

age indicator results, ASH-P remains superior. In summary, for real-world OOD detection with Skeleton-OOD, the ASH-P method is recommended for optimal results.

In addition, by comparing the results of our method across the three ASH strategies with those of the pure post-hoc ASH strategy, it is evident that incorporating this feature activation operation during the training stage can enhance the model’s OOD detection capability to some extent. For instance, as shown in Table 2, the ASH-P baseline in the fifth row compared to our Ours-ASH-P in the third to last row demonstrates varying degrees of improvement in most indicators across the three datasets. Furthermore, Table 3 illustrates that this approach even slightly enhances the model’s recognition accuracy for ID data.

It can be observed that compared to the first two datasets, the overall prediction accuracy on Kinetics is not satisfactory. Additionally, the direct classification results on the ID dataset are relatively poor. By comparing the incorrectly predicted samples on the Kinetics data set, we discover that some ID samples are misclassified as OOD samples, which means that the model lacks confidence in the ID samples. This also shows to some extent that the data itself may lack expressive power, which prevents the model itself from learning more distinguishing features. One possible reason could be attributed to the graph construction as shown in Figure 2. Firstly, the Kinetics dataset itself includes a large number of actions involving interactions between people and objects, making it difficult to distinguish using skeleton data only. Secondly, through our visualization analysis, there are certain issues in extracting Kinetics nodes in the STGCN [1]. For instance,

nodes 15 and 16 in the data represent the left and right eyes respectively. However, these nodes may not provide much information about the actions. Moreover, while the dataset models the left and right hips separately, it lacks crucial information about the key body waist nodes, which are essential for understanding the type of limb movement. **In summary, our method outperforms others in certain indicators for some datasets of ID samples and significantly surpasses existing methods in OOD samples. This addresses our primary challenge of enhancing OOD detection capabilities while maintaining ID recognition accuracy.**

4.3.2. Number of dimensions for OOD representation

Using machine learning methods to process categorical data generally requires one-hot encoding of category labels in the data. The processed vectors are then input into the model to participate in training. The dimension of the encoding vector is generally equal to the total number of data categories. In our work, to make the model realize that there are other unknown categories besides the ID category, an additional k -dimensional vector is concatenated to mark whether the data belongs to OOD. The experimental results on the NTU60 dataset are shown in Table 4.

The last two rows indicate the results that we use additional dimensions ($k = 1$ and $k = 3$) in the embedding to represent OOD samples. Since the training set consists only of ID samples, there are no samples with these extra dimensions set to 1. We hope this operation can effectively inform the model during training that all samples belong to the first 55 classes and not to the 56th class or the 56th-58th classes, providing it with extra information. By comparing the results in the table for the rows "55", "58 (55+3)", and "56 (55+1)", it can be observed that using the additional dimension indeed improves the model's accuracy of OOD detection. This further validates the effectiveness of our design.

Table 4: Ablation experiment results reflect the performance of each module. The bold numbers represent the best performance.

NTU60	Unseen			Seen	
	Error ↓	FPR95 ↓	AUROC ↑	Top1 ↑	Overlap ↓
55	34.58	64.16	83.57	91.59	0.41
58 (55+3)	33.49	61.99	85.66	91.49	0.41
56 (55+1)	30.42	52.68	86.64	91.94	0.39

At the same time, comparing the results using 56(55+1) and 58(55+3) dimensions, reveals that using an extra 1 dim is more effective than that of 3 dims. Perhaps it is because higher-dimensional representations can easily cause information redundancy, which makes training difficult. Therefore, the experimental results in this paper all use additional 1-dimensional vectors to represent the OOD classes. It should be noted that perhaps it would be better to use more dimensional representations for the NTU120 and Kinetics400 datasets, but the 1-dimensional OOD representation method is used here for the requirement of comparison.

4.3.3. Other loss functions for OOD detection

To evaluate the effectiveness of the proposed energy-based loss function, we compare it with another method LogitNorm [41]. Experiments here use our proposed workflow, with the only difference being the use of two different training loss functions. Results for both OOD detection and ID recognition tasks are shown in Table 5 and Table 6, respectively.

Table 5: Results on ID-OOD mix dataset trained with LogitNorm loss function. The best results of each column are in bold.

OOD	NTU60			NTU120			Kinetics400			Average		
Methods	Error ↓	FPR95 ↓	AUROC ↑	Error ↓	FPR95 ↓	AUROC ↑	Error ↓	FPR95 ↓	AUROC ↑	Error ↓	FPR95 ↓	AUROC ↑
LogitNorm ASH-P	34.33	63.66	78.22	30.75	56.50	84.57	51.23	88.73	52.69	38.77	69.63	71.83
LogitNorm ASH-S	39.11	73.21	76.50	41.09	77.19	75.01	51.39	96.74	46.55	43.86	82.38	66.02
LogitNorm ASH-B	43.10	81.21	75.05	32.85	60.71	86.70	51.46	94.69	52.70	51.09	96.10	51.31

Table 6: Results on ID-only test dataset trained with LogitNorm loss function. The best results of each column are in bold.

ID-only	NTU60		NTU120		Kinetics400		Average	
Methods	Top1 ↑	Overlap ↓	Top1 ↑	Overlap ↓	Top1 ↑	Overlap ↓	Top1 ↑	Overlap ↓
LogitNorm ASH-P	90.66	0.37	89.05	0.47	26.30	0.92	68.67	0.59
LogitNorm ASH-S	90.39	0.59	88.17	0.64	21.39	0.93	66.76	0.65
LogitNorm ASH-B	4.44	0.79	17.63	0.79	26.19	0.91	16.09	0.83

By comparison, it can be seen that in most experiments, the model trained with our proposed energy-based loss function outperforms the results obtained with LogitNorm. It can also be observed that the results trained with LogitNorm show significant variation among different activation methods, particularly with the ASH-B method. We speculate that this may be because

the LogitNorm method itself is a correction approach based on the original softmax prediction activation. Moreover, our designed framework partly uses ASH to activate the skeleton features and then applies the LogitNorm loss function for correction. This may lead to either insignificant effects (as seen in LogitNorm-ASH-P and LogitNorm-ASH-S) or overcorrection (as seen in LogitNorm-ASH-B). On the other hand, our framework utilizes ASH for feature activation, and during the training stage, the proposed loss function directly reinforces the learning of the OOD discrimination target through energy distance. The experimental results also show that for our framework, using this target-enhancing training method during the training stage through loss function is more effective. Therefore, overall, our framework not only addresses the issue of OOD feature extraction from the perspective of feature activation but also strengthens the range of ID sample energy scores from the perspective of the energy value distribution with the aim of discrimination. This multi-angle approach enables the model to address both OOD and ID sample recognition problems effectively.

4.3.4. Ablation study

Table 7: Ablation experiment results reflect the performance of each module. The bold numbers represent the best performance.

NTU60	OOD			ID	
	Error ↓	FPR95 ↓	AUROC ↑	Top1 ↑	Overlap ↓
GCN	49.31	93.61	48.37	7.24	0.89
ASH	34.33	63.66	78.22	90.66	0.59
CE Loss	37.51	70.02	79.58	91.61	0.49
ours	30.42	52.68	86.64	91.94	0.39

- Effect of Activation Shaping:** Comparing the results of the GCN with ours, it shows that with the help of the ASH strategy, the Error metric decreases by 58.59%. AUROC accuracy also improves by 79.12%. ASH can significantly improve the OOD recognition ability of the model. At the same time, it can be seen from the table that the seen accuracy in the GCN experiment is very low because the energy score distribution of unseen and seen has a high degree of overlap. Therefore, many ID samples will be misidentified as OOD. The OOD detection method that uses the energy score of the ranked 10% ID sam-

ple as the threshold in OOD detection is suspected of overcorrecting the performance of this model.

- Effect of Feature Fusion Block:** Comparing it to the column ASH, leveraging typical GCN embeddings results in an 11.39% increase in the Error metric and an 8.42 percentage increase in AUROC accuracy. When considering the experimental outcomes from the GCN scenario, it becomes evident that the feature fusion module empowers the model to increase the accuracy of out-of-distribution (OOD) detection without compromising its ability to recognize in-distribution (ID) samples.

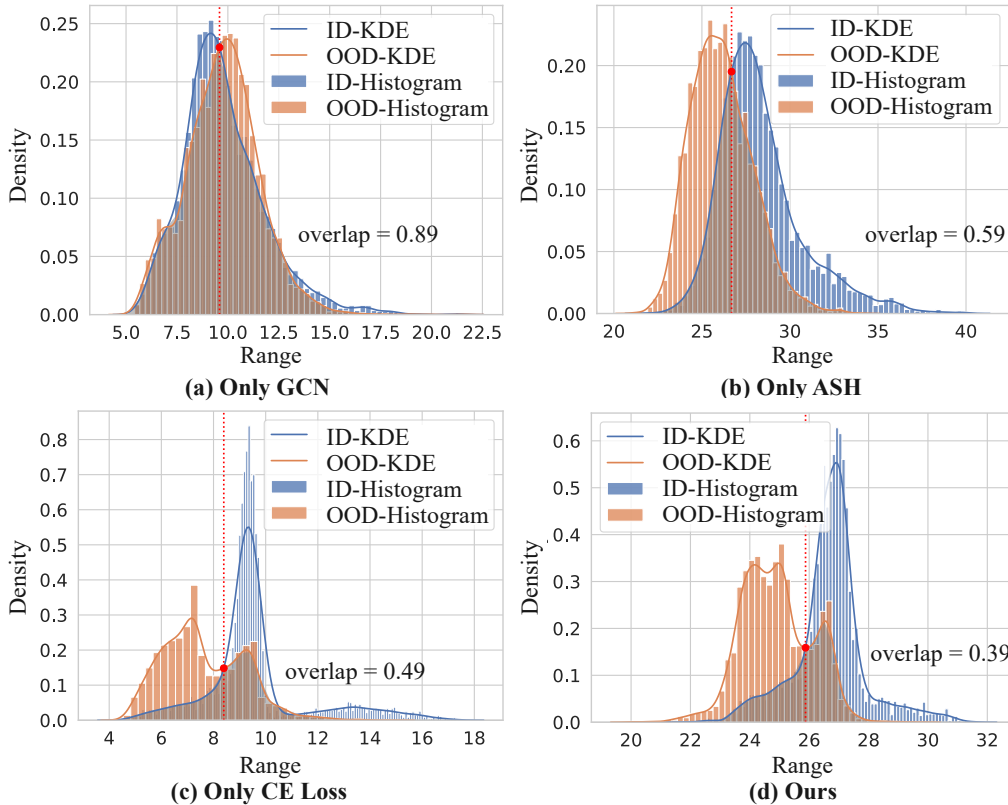


Figure 5: Distributions of ID and OOD samples among different ablation studies. The blue area indicates the ID distribution, and the orange shows the OOD samples. The value of overlap represents the amount of overlapping area between the two distributions.

- Effect of Energy Loss:** Comparing the results with only traditional cross-entropy loss (bottom two rows), it can be observed that the

method utilizing energy loss employed in this paper significantly enhances the model’s capabilities across various settings. Additionally, we discover that compared with directly employing ASH, the model trained with the feature fusion module but using only cross-entropy loss performs less effectively on OOD tasks, but slightly outperforms in ID classification. This further indicates that the combined use of the feature fusion module and energy loss can address the overall capabilities of the model, leading to better differentiation between in-distribution and out-of-distribution data.

- **The impact of different model components on energy score distribution:** From Figure 5, it can be observed that incorporating the ASH method during the training stage (Figure 5 (b)) reduces the range of energy score distribution compared to the pure GCN model. Additionally, it creates the distance between the two distribution peaks. Contrasting Figure 5 (b) with Figure 5 (d), where the only difference lies in the usage of a feature fusion block, shows a further reduction in the distribution range from 20 to 12. Moreover, the variance of the ID data is also diminished. Furthermore, as evident from Figure 5 (c) and (d), adjustments to the Energy-based loss function result in not only a decreased range of the data but also a reduction in the variance of the OOD data. The combination of these effects minimizes the overlap area of the ID and OOD distributions in our model test results.

4.3.5. Different pruning percentages

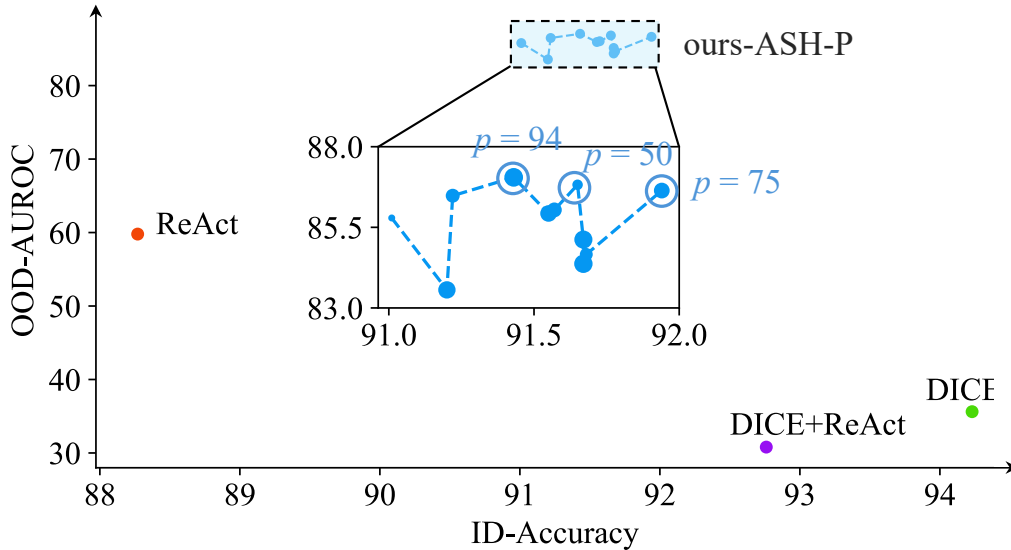


Figure 6: ID-OOD tradeoff on the NTU-RGB+D 60 dataset. The size of the points in the enlarged line chart corresponds to different p values. The line chart represents the results of our method for p -values in the range of 40%-90%.

To explore the effect of pruning percentage p , different values are tested in our experiments. As shown in Figure 6, we select the best-performing ASH-P strategy on the NTU60 dataset for evaluation. The size of the blue points reflects the pruning percentage p . The red, green, and purple points respectively represent the performance of the ReAct, DICE, and DICE+ReAct methods at their optimal ratios.

The data points located closer to the upper-right corner of the figure exhibit superior performance. Our approach achieves optimal results when integrated with the ASH strategy. Concerning the OOD detection task across various p values, it is apparent that the correlation between accuracy and p value is nonlinear. To balance the accuracy between OOD and ID samples, we choose the p -value of 75 as the best pruning percentage.

4.3.6. Different backbones of skeleton feature extractor

As stated in Section 1, we focus on exploiting the extracted features to extend their adaptability for OOD detection while maintaining robust prediction performance for the supervised classes. Thus, we use the state-of-the-art

Table 8: Results on ID-OOD mix dataset with three different extractors. The best results of each method are in bold. “+” indicates an increase in the corresponding indicator value, while “-” indicates a decrease.

OOD Methods	NTU60			NTU120			Kinetics400		
	Error ↓	FPR95 ↓	AUROC ↑	Error ↓	FPR95 ↓	AUROC ↑	Error ↓	FPR95 ↓	AUROC ↑
ST-GCN-only	35.00	65.01	81.16	56.07	68.36	53.85	51.37	95.11	51.79
InfoGCN-only	34.43	66.80	80.29	52.39	66.94	59.07	-	-	-
EfficientGCN-only	35.84	67.02	79.86	54.92	67.82	58.92	-	-	-
ST-GCN ASH-P	-2.53	-5.06	+18.08	-4.39	+3.13	+18.08	+0.53	-2.38	+5.10
ST-GCN ASH-S	+1.83	+3.66	-4.53	-23.11	-7.43	+29.05	+0.45	-2.02	+3.06
ST-GCN ASH-B	+8.10	+16.20	-6.11	-23.22	-7.65	+32.85	+0.55	-2.44	+5.29
InfoGCN ASH-P	-1.08	-0.88	+4.60	-23.22	+1.44	+28.65	-	-	-
InfoGCN ASH-S	-0.23	-0.06	+2.04	-9.02	+3.34	+20.75	-	-	-
InfoGCN ASH-B	+0.36	+1.18	-3.36	-11.52	-0.02	+24.49	-	-	-
EfficientGCN ASH-P	+4.44	+5.35	+1.46	-11.00	+0.56	+22.06	-	-	-
EfficientGCN ASH-S	-1.02	+1.90	+0.87	-15.63	-3.53	+22.28	-	-	-
EfficientGCN ASH-B	+7.05	+11.50	-1.12	-16.63	-3.99	+23.27	-	-	-

supervised skeleton-based recognition model HD-GCN as a feature extractor. Additionally, we also select ST-GCN, InfoGCN [42] and EfficientGCN [43], which are similar frameworks as HD-GCN in classic action recognition tasks, to serve as a feature extractor for comparative experiments. The results demonstrate that the model with HD-GCN still outperforms many other baselines.

Table 9: Results on ID-only dataset with three different extractors. The best results of each method are in bold. “+” indicates an increase in the corresponding indicator value, while “-” indicates a decrease.

ID-only Methods	NTU60		NTU120		Kinetics400	
	Top1 ↑	Overlap ↓	Top1 ↑	Overlap ↓	Top1 ↑	Overlap ↓
ST-GCN-only	90.33	0.53	48.11	0.81	24.03	0.92
InfoGCN-only	90.95	0.51	73.64	0.76	-	-
EfficientGCN-only	90.88	0.55	63.21	0.79	-	-
ST-GCN ASH-P	+0.64	-0.10	+40.88	-0.09	-2.10	-0.03
ST-GCN ASH-S	-0.25	+0.03	+40.70	-0.35	-2.64	+0.01
ST-GCN ASH-B	+0.08	+0.08	+39.86	-0.40	-2.49	-0.03
InfoGCN ASH-P	+0.92	-0.04	+15.30	-0.08	-	-
InfoGCN ASH-S	-0.01	-0.01	+15.38	-0.08	-	-
InfoGCN ASH-B	-0.20	+0.07	+15.60	-0.23	-	-
EfficientGCN ASH-P	+0.35	-0.13	+24.71	-0.32	-	-
EfficientGCN ASH-S	+0.14	-0.11	+25.22	-0.27	-	-
EfficientGCN ASH-B	-0.09	-0.02	+25.51	-0.22	-	-

It should be noted that we use the Kinetics400 dataset processed by the work ST-GCN [1], while the model InfoGCN and EfficientGCN are designed

for motion stream data, so the results on this dataset are missing.

Compared with the results in Table 2 and Table 8, the three feature extractor backbones perform less effectively than Skeleton-OOD on the either OOD or ID recognition task. This result indicates that HD-GCN has a stronger capability as a feature extractor than these three. This aligns with findings from numerous existing studies in the field of action recognition, which show that HD-GCN holds the state-of-the-art performance [23]. This further confirms that a superior feature extractor significantly aids in improving OOD recognition. The reason for this phenomenon may not only be related to the design of the network structure, but more importantly, the graph structures used by the methods are different.

Also, comparing the results of each backbone and the below activation-added methods in Table 8 and Table 9, it can be concluded that adding activation operations after the feature extractor can indeed improve the OOD detection capability of the model. This is not only limited to HD-GCN as an extractor but also works on models with other structures.

4.3.7. Detection result analysis and visualization

Based on the performance of the train and test sets of NTU-RGB+D 60, the energy distribution in the test set is bimodal. We suspect that some out-of-distribution classes are similar to in-distribution classes, making them difficult to distinguish. We list these ‘confusing’ classes in Table 10.

Table 10: Misclassification statistics

Wrong number	533	73	48	93	96	50
ID classes	clapping	giving object	wipe face	headache	fan self	pat on back
OOD classes	hand waving, kicking something, rubbing two hands, neck pain, touch pocket					

Table 10 lists out the count of samples and their class names respectively from OOD samples that are misclassified into ID classes. Upon examining the class names, it is apparent that certain actions have subtle distinctions but are still similar, such as ‘clapping’ and ‘hand waving’, or ‘pat on back’ and ‘neck pain’ as shown in Figure 7. How the model captures the little differences between these actions still needs some improvement.

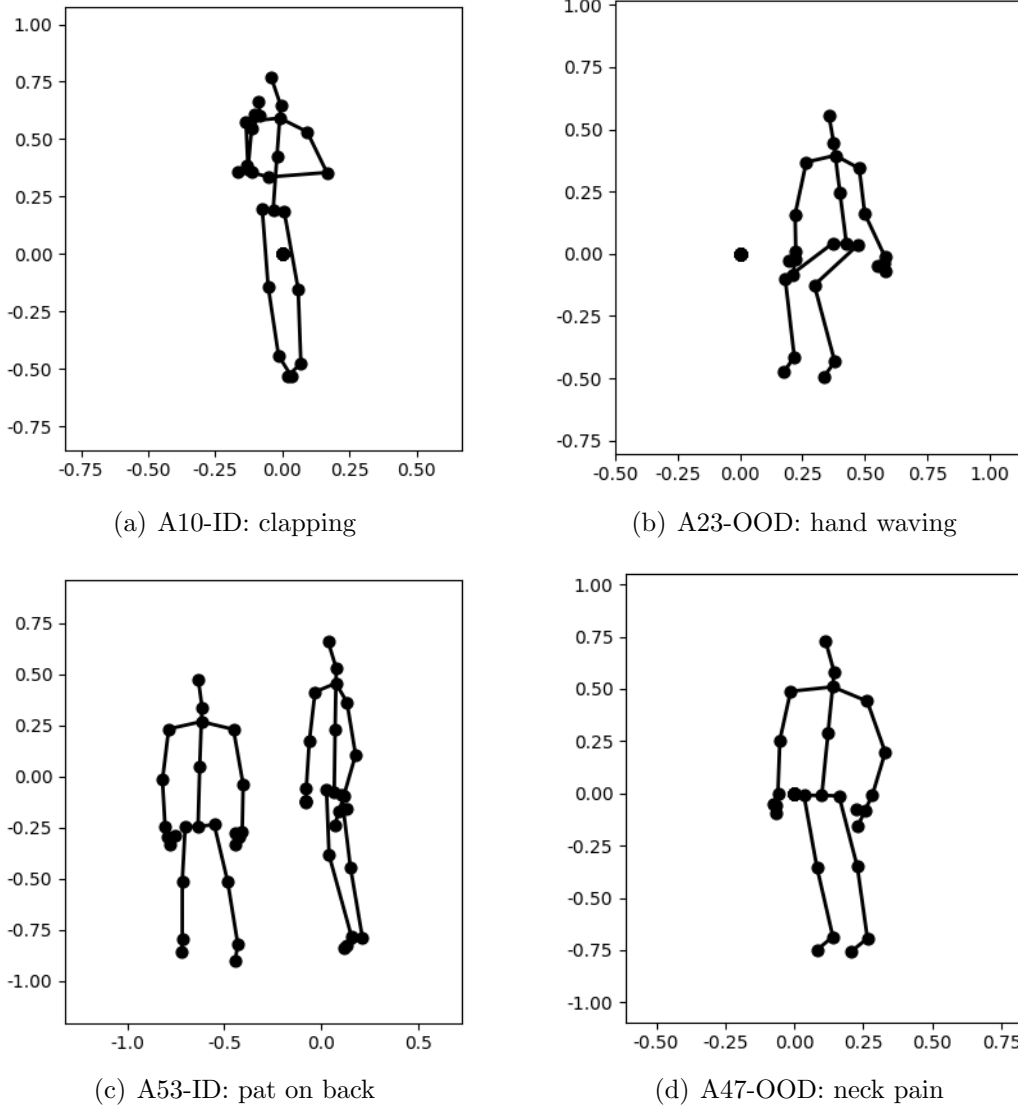


Figure 7: Example of correct classified ID samples and misclassified OOD samples.

4.3.8. Randomly joint masking result

In order to test the scalability of the model on multiple tasks, we also considered the results of the recognition and classification problems with missing node information in reality. The results of ID and OOD detection on the NTU60 data are shown in Table 11. And plot the trend of AUROC

and TOP1 results as shown in Figure 8.

Table 11: Test results of different joint mask percentages (p). Using our model (ASH-P), we randomly masked different percentages of joint information on the NTU-RGB+D 60 ID-OOD mix dataset.

	OOD			ID	
	ERROR ↓	FPR95 ↓	AUROC ↑	Top1 ↑	Overlap ↓
origin(0)	30.42	52.68	86.64	91.94	0.39
$p=5\%$	33.99	52.32	73.97	47.29	0.46
$p=7\%$	33.56	53.27	73.62	46.58	0.46
$p=10\%$	33.74	52.86	75.30	46.06	0.49
$p=15\%$	33.72	52.91	75.51	45.19	0.49
$p=20\%$	33.98	52.33	76.06	44.82	0.49
$p=30\%$	34.18	51.90	76.03	44.05	0.49
$p=50\%$	34.11	52.04	75.34	43.91	0.49
$p=70\%$	34.32	51.60	75.36	43.88	0.49

From the results we can clearly see that randomly masking on joints affects the accuracy of the ID data most, but slightly on OOD samples. Especially when the percentage is small, the OOD result is not just a simple downward trend. This may be related to the position of the nodes randomly masked.

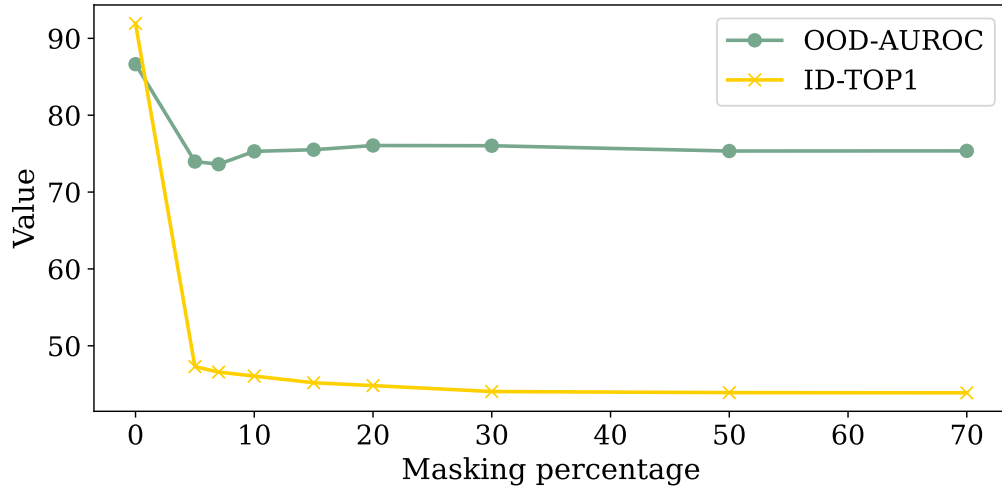


Figure 8: Results of ID and OOD performance under different masking percentages.

5. Conclusion and future works

This paper introduces Skeleton-OOD, an end-to-end framework designed to address the challenge of recognizing out-of-distribution human action samples. The framework adopts a hierarchical graph composition method and utilizes GCN to extract the feature maps of human skeletons. Subsequently, a feature activation strategy is applied and we fuse the activated features with the original ones through a proposed feature fusion block. Experiments show that this step equips the model with the innate ability to identify out-of-distribution data while maintaining its capability for ID classification. Next, an energy score is computed for each test sample based on the logits output by the classifier. This helps determine whether it belongs to an OOD category. The model is trained using a designed energy-based loss function, designed to reduce the variance of ID data and differentiate between ID and OOD samples. Experimental results demonstrate that this approach effectively mitigates the overconfidence issue encountered by human action classification models when dealing with samples beyond the training category. Notably, since the model training process relies exclusively on sample information within the branch, without prior knowledge of OOD distribution characteristics, it exhibits broad practical applicability.

Admittedly, the model still has some potential limitations. Firstly, since the model is trained on GCN, its generalization ability is constrained by the number of skeleton nodes across various datasets. In real-world scenarios, if the trained model is deployed to identify whether a test sample with a different number of nodes is out-of-distribution, its accuracy may be compromised. Secondly, the end-to-end model’s generalization capability is still bounded by the model parameters and the size of the dataset. The way the activation method is used during training causes some of the improvement in results to come from the training operation. One potential solution is to explore semi-supervised learning techniques to mitigate this issue. Moreover, the problem can be further addressed by introducing generative models and conducting training on datasets with limited ID samples. By leveraging existing category text and feature information, the model can infer the name of the unknown category for unfamiliar sample features. In summary, human action recognition tasks present diverse application scenarios, with numerous novel challenges awaiting exploration based on specific practical contexts.

Appendix A. Appendix

Appendix A.1. Three different activation shaping strategies

In our paper, we try three different activation shaping strategies and compare the results respectively. Here are their implementation details in Table A.12.

Table A.12: Detailed activation shaping algorithms

Algorithm S1. Activation shaping algorithms		
Input: Feature maps F ;		
Pruning percentage p ;		
Output: Modified feature maps F_P , F_B , or F_S ;		
ASH-P: Activation Shaping with Pruning	ASH-B: Activation Shaping with Binarizing	ASH-S: Activation Shaping with Scaling
1: $t = p \times \text{rank}(F)$ 2: $F_P[\text{idx}(F < t)] = 0$ 3: return F_P	1: $t = p \times \text{rank}(F)$ 2: $s = \text{sum}(F)$ 3: $F_B[\text{idx}(F < t)] = 0$ 4: $n = \text{len}(\text{idx}(F \neq 0))$ 5: $F_B[F \neq 0] = s/n$ 6: return F_B	1: $t = p \times \text{rank}(F)$ 2: $s1 = \text{sum}(F)$ 3: $F_P[\text{idx}(F < t)] = 0$ 4: $s2 = \text{sum}(F)$ 5: $F_S = F[\text{idx}(F \neq 0)] \times \exp(s1/s2)$ 6: return F_S

References

- [1] S. Yan, Y. Xiong, D. Lin, Spatial temporal graph convolutional networks for skeleton-based action recognition, in: Proceedings of the AAAI conference on artificial intelligence, volume 32, 2018.
- [2] Y. Chen, Z. Zhang, C. Yuan, B. Li, Y. Deng, W. Hu, Channel-wise topology refinement graph convolution for skeleton-based action recognition, in: Proceedings of the IEEE/CVF international conference on computer vision, 2021, pp. 13359–13368.
- [3] K. Cheng, Y. Zhang, C. Cao, L. Shi, J. Cheng, H. Lu, Decoupling gen with dropgraph module for skeleton-based action recognition, in: Computer Vision–ECCV 2020: 16th European Conference, Glasgow, UK, August 23–28, 2020, Proceedings, Part XXIV 16, Springer, 2020, pp. 536–553.
- [4] Y. Yu, S. Shin, M. Ko, K. Lee, Exploring using jigsaw puzzles for out-of-distribution detection, Computer Vision and Image Understanding (2024) 103968.
- [5] E. Nalisnick, A. Matsukawa, Y. W. Teh, D. Gorur, B. Lakshminarayanan, Do deep generative models know what they don’t know? (2019).

- [6] A. Geiger, P. Lenz, R. Urtasun, Are we ready for autonomous driving? the kitti vision benchmark suite, in: 2012 IEEE conference on computer vision and pattern recognition, IEEE, 2012, pp. 3354–3361.
- [7] T. Schlegl, P. Seeböck, S. M. Waldstein, U. Schmidt-Erfurth, G. Langs, Unsupervised anomaly detection with generative adversarial networks to guide marker discovery, in: International conference on information processing in medical imaging, Springer, 2017, pp. 146–157.
- [8] D. Hendrycks, K. Gimpel, A baseline for detecting misclassified and out-of-distribution examples in neural networks, Proceedings of International Conference on Learning Representations (2017).
- [9] A. Nguyen, J. Yosinski, J. Clune, Deep neural networks are easily fooled: High confidence predictions for unrecognizable images, in: Proceedings of the IEEE conference on computer vision and pattern recognition, 2015, pp. 427–436.
- [10] Y. Sun, C. Guo, Y. Li, React: Out-of-distribution detection with rectified activations, in: Advances in Neural Information Processing Systems, 2021.
- [11] Y. Zhu, Y. Chen, C. Xie, X. Li, R. Zhang, H. Xue, X. Tian, Y. Chen, et al., Boosting out-of-distribution detection with typical features, Advances in Neural Information Processing Systems 35 (2022) 20758–20769.
- [12] Q. Wu, et al., Energy-based out-of-distribution detection for graph neural networks, in: International Conference on Learning Representations (ICLR), 2023.
- [13] J. Koo, S. Choi, S. Hwang, Generalized outlier exposure: Towards a trustworthy out-of-distribution detector without sacrificing accuracy, Neurocomputing 577 (2024) 127371.
- [14] A. Djuricic, et al., Extremely simple activation shaping for out-of-distribution detection (2023).
- [15] A. S. Nikam, A. G. Ambekar, Sign language recognition using image based hand gesture recognition techniques, in: 2016 Online International Conference on Green Engineering and Technologies (IC-GET), 2016.

- [16] Y.-G. Jiang, Q. Dai, W. Liu, X. Xue, C.-W. Ngo, Human action recognition in unconstrained videos by explicit motion modeling, *IEEE Transactions on Image Processing* 24 (2015) 3781–3795.
- [17] G. Chéron, I. Laptev, C. Schmid, P-cnn: Pose-based cnn features for action recognition, in: *Proceedings of the IEEE international conference on computer vision*, 2015, pp. 3218–3226.
- [18] M. Liu, H. Liu, C. Chen, Enhanced skeleton visualization for view invariant human action recognition, *Pattern Recognition* 68 (2017) 346–362.
- [19] K. Simonyan, A. Zisserman, Two-stream convolutional networks for action recognition in videos, *Advances in neural information processing systems* 27 (2014).
- [20] H. Wang, L. Wang, Modeling temporal dynamics and spatial configurations of actions using two-stream recurrent neural networks, in: *Proceedings of the IEEE conference on computer vision and pattern recognition*, 2017, pp. 499–508.
- [21] J. Liu, G. Wang, P. Hu, L.-Y. Duan, A. C. Kot, Global context-aware attention lstm networks for 3d action recognition, in: *Proceedings of the IEEE conference on computer vision and pattern recognition*, 2017, pp. 1647–1656.
- [22] H. Tian, Y. Zhang, H. Wu, X. Ma, Y. Li, Multi-scale sampling attention graph convolutional networks for skeleton-based action recognition, *Neurocomputing* (2024) 128086.
- [23] J. Lee, M. Lee, D. Lee, S. Lee, Hierarchically decomposed graph convolutional networks for skeleton-based action recognition, in: *Proceedings of the IEEE/CVF International Conference on Computer Vision*, 2023, pp. 10444–10453.
- [24] Y. Sun, Y. Li, Dice: Leveraging sparsification for out-of-distribution detection, in: *European Conference on Computer Vision*, 2022.
- [25] X. Liu, Y. Lochman, C. Zach, Gen: Pushing the limits of softmax-based out-of-distribution detection, in: *Proceedings of the IEEE/CVF*

- Conference on Computer Vision and Pattern Recognition, 2023, pp. 23946–23955.
- [26] D. Hendrycks, S. Basart, M. Mazeika, A. Zou, J. Kwon, M. Mostajabi, J. Steinhardt, D. Song, Scaling out-of-distribution detection for real-world settings, International Conference on Machine Learning (2022).
 - [27] Y. Song, N. Sebe, W. Wang, Rankfeat: Rank-1 feature removal for out-of-distribution detection, Advances in Neural Information Processing Systems 35 (2022) 17885–17898.
 - [28] J. Zhang, et al., Openood v1. 5: Enhanced benchmark for out-of-distribution detection, arXiv preprint arXiv:2306.09301 (2023).
 - [29] M. Hein, M. Andriushchenko, J. Bitterwolf, Why relu networks yield high-confidence predictions far away from the training data and how to mitigate the problem, in: Proceedings of the IEEE/CVF conference on computer vision and pattern recognition, 2019, pp. 41–50.
 - [30] Y. LeCun, S. Chopra, R. Hadsell, M. Ranzato, F. Huang, A tutorial on energy-based learning, Predicting structured data 1 (2006).
 - [31] T. N. Kipf, M. Welling, Semi-supervised classification with graph convolutional networks, in: International Conference on Learning Representations (ICLR), 2017.
 - [32] J. Hu, L. Shen, G. Sun, Squeeze-and-excitation networks, in: Proceedings of the IEEE conference on computer vision and pattern recognition, 2018, pp. 7132–7141.
 - [33] W. Yu, et al., Metaformer is actually what you need for vision, in: IEEE Conference on Computer Vision and Pattern Recognition, 2022, pp. 10819–10829.
 - [34] A. Shahroudy, J. Liu, T.-T. Ng, G. Wang, Ntu rgb+ d: A large scale dataset for 3d human activity analysis, in: Proceedings of the IEEE conference on computer vision and pattern recognition, 2016, pp. 1010–1019.

- [35] J. Liu, A. Shahroudy, M. Perez, G. Wang, L.-Y. Duan, A. C. Kot, Ntu rgb+ d 120: A large-scale benchmark for 3d human activity understanding, *IEEE transactions on pattern analysis and machine intelligence* 42 (2019) 2684–2701.
- [36] W. Kay, J. Carreira, K. Simonyan, B. Zhang, C. Hillier, S. Vijayanarasimhan, F. Viola, T. Green, T. Back, P. Natsev, et al., The kinetics human action video dataset, *arXiv preprint arXiv:1705.06950* (2017).
- [37] K. He, X. Zhang, S. Ren, J. Sun, Deep residual learning for image recognition, in: *Proceedings of the IEEE conference on computer vision and pattern recognition*, 2016, pp. 770–778.
- [38] S. Liang, Y. Li, R. Srikant, Enhancing the reliability of out-of-distribution image detection in neural networks (2019).
- [39] J. Davis, M. Goadrich, The relationship between precision-recall and roc curves, in: *Proceedings of the 23rd international conference on Machine learning*, 2006, pp. 233–240.
- [40] C. Zhao, D. Du, A. Hoogs, C. Funk, Open set action recognition via multi-label evidential learning, in: *Proceedings of the IEEE/CVF Conference on Computer Vision and Pattern Recognition*, 2023, pp. 22982–22991.
- [41] H. Wei, R. Xie, H. Cheng, L. Feng, B. An, Y. Li, Mitigating neural network overconfidence with logit normalization, in: *International conference on machine learning*, PMLR, 2022, pp. 23631–23644.
- [42] H.-g. Chi, M. H. Ha, S. Chi, S. W. Lee, Q. Huang, K. Ramani, Infogen: Representation learning for human skeleton-based action recognition, in: *Proceedings of the IEEE/CVF Conference on Computer Vision and Pattern Recognition (CVPR)*, 2022, pp. 20186–20196.
- [43] Y.-F. Song, Z. Zhang, C. Shan, L. Wang, Constructing stronger and faster baselines for skeleton-based action recognition, *IEEE transactions on pattern analysis and machine intelligence* 45 (2022) 1474–1488.